

Temporal-Spatial Feature Pyramid for Video Saliency Detection

Qinyao Chang ^{*} Shiping Zhu ^{*} Lanyun Zhu

Beihang University, 100191 Beijing, China.

{changqinyao, shiping.zhu, zhulanyun}@buaa.edu.cn

Abstract

In this paper, we propose a 3D fully convolutional encoder-decoder architecture for video saliency detection, which combines scale, space and time information for video saliency modeling. The encoder extracts multi-scale temporal-spatial features from the input continuous video frames, and then constructs temporal-spatial feature pyramid through temporal-spatial convolution and top-down feature integration. The decoder performs hierarchical decoding of temporal-spatial features from different scales, and finally produces a saliency map from the integration of multiple video frames. Our model is simple yet effective, and can run in real time. We perform abundant experiments, and the results indicate that the well-designed structure can improve the precision of video saliency detection significantly. Experimental results on three purely visual video saliency benchmarks and six audio-video saliency benchmarks demonstrate that our method achieves state-of-the-art performance.

1. Introduction

Video saliency detection aims to predict the point of fixation for the human eyes while watching videos freely. It is widely applied in a lot of areas such as video compression [17, 43], video surveillance [15, 42] and video captioning [31].

Most of existing video saliency detection models employ the encoder-decoder structure, and rely on the temporal recurrence to predict video saliency. For example, ACLNet [39] encodes static saliency features through attention mechanism, and then learns dynamic saliency through ConvLSTM [36]. SalEMA [25] uses exponential moving average instead of LSTM to extract temporal features for video saliency detection. SalSAC [40] proposes a correlation-based ConvLSTM to balance the alteration of



Figure 1. The visualization of video saliency results of two different videos (interval of 30 frames)

saliency caused by the change of image characteristics of past frame and current frame. However, such a saliency modeling approach has the following problems. Firstly, the spatial saliency model is pretrained on the static image saliency datasets before finetuning on the video saliency datasets. However, the effectiveness of this transfer learning mechanism may be limited, since the resolutions of two datasets are different while saliency is greatly influenced by the image shape. Secondly, restricted by memory, the training of video saliency model requires to extract continuous video frames from the datasets randomly. However, the approach based on LSTM needs to utilize backpropagation through time to predict the video saliency of each frame. In this way, the state of LSTM of the first frame for the selected clip must be void, while, during the test, only the state of the LSTM of the first frame of the video is void, such discrepancy makes the modeling of method based on LSTM insufficient. Thirdly, as mentioned by [28], all the methods based on LSTM overlay the temporal information on top of spatial information, and fail to utilize both kinds of information at the same time, which is crucial for video saliency detection.

To alleviate above problems, some methods [28, 38, 4] employ 3D convolutions to continuously aggregate the temporal and spatial clues of videos. While they achieve out-

^{*}Corresponding Author.

standing performance, there still remains an important issue, that is, lacking the utilization of multi-level features. Multi-level features are essential for the task of saliency detection, since the human visual mechanism is complicated and the concerned region is determined by various factors and from multiple levels. For example, some large objects may be salient, which are captured from the deeper layers with a relatively large receptive fields. Some small but moving at a high speed objects are also salient, which are captured from shallower layers holding more low-level information. Some GRU- and LSTM-based methods [40, 23] fusing multi-level features from different layers have achieved great success, demonstrating the effectiveness of this mechanism. However, how to combine the effective 3D convolutions with this mechanism is still unexplored.

In order to solve the past problems, we propose a new 3D fully convolutional encoder-decoder architecture for video saliency detection, the generated saliency maps of video frames are shown in Figure 1. We fully consider the influence of time, space and scale and establish a temporal-spatial feature pyramid. Meanwhile, the temporal-spatial semantic features of deep layer are aggregated to each layer of the pyramid. In view of the different receptive fields of temporal dimension for the features of various layers, we separately perform independent hierarchical decoding on different levels of the feature pyramid to fully take the effect of temporal-spatial saliency features with various scales into consideration. Since the unpooling layer shall be bound together with the maxpooling layer, the decoder network cannot be designed freely. Refer to the recent studies on the semantic segmentation of 2D network, the convolution with the upsampling in decoder [7, 8, 9, 10, 24] can obtain better result, compared with the previous method, which adopted the deconvolution or unpooling [2, 26, 34]. We put away the previous deconvolution and unpooling operation of 3D fully convolutional encoder-decoder [28] and completely adopt the 3D convolution and the trilinear upsampling.

At the same time, in order to predicting audio-video saliency, audio information and visual information are fused, and the obtained features are integrated on the original visual network in the form of attention. Our network is simple in structure, lower in parameters, and higher in prediction precision, which has obvious difference with other methods of the state-of-the-art. Our method ranks first in the largest and most diverse video saliency dataset, such as DHF1K [39].

The main contributions of the paper are as following:

We develop a new 3D fully convolutional temporal-spatial feature pyramid network called TSFP-Net, which completely consists of 3D convolution and trilinear upsampling and put away the limited network design of unpooling layer and deconvolution layer.

We construct feature pyramid of different scales contain-

ing rich temporal-spatial semantic features, and build a hierarchical 3D convolutional decoder to decode. We prove that such approach can significantly improve the detection performance of the video saliency. By fusing audio information and visual information and integrating them into the original visual network in the form of attention, we can simultaneously perform audio-video saliency prediction through TSFP-Net (with audio).

We evaluate our model on three purely visual large-scale video saliency datasets and six audio-video saliency datasets, comparing with the state-of-the-art methods, our model can achieve enormous gains.

2. Ralated Work

The video saliency detection consists of multiple directions, which mainly can be divided into two categories, fixation prediction and salient object detection. Fixation prediction aims to model the probability that the human eyes pay attention to each pixel while watching video images, the preparation of such dataset usually needs to recruit many volunteers and an eye tracker is used to record the gaze position of each volunteer when they watch video freely. Salient object detection aims to segment the accurate contours of the objects of interest of the human eyes in the video images, and the dataset shall be manually marked so as to obtain the accurate segmentation edges of the salient objects. We focus on the fixation prediction in this paper.

2.1. The Latest 2D Video Saliency Detection Networks

In the past, most video saliency detection methods predicted the saliency map by adding temporal recurrence module to the static network. DeepVS[20] establishes a sub-network of objects through YOLO [32] and build up a sub-network of motion through FlowNet [13], then, convey the obtained spatial-temporal features to the double-layer ConvLSTM for prediction. ACLNet [39] adopts a attention module and a ConvLSTM module to construct the network, among which, the attention module is trained on the large static saliency dataset SALICON [18] and the ConvLSTM module is trained on the video saliency dataset, the final model is obtained through the alternating training of static and dynamic saliency. SalEMA [25] discusses the performance of exponential moving average (EMA) and ConvLSTM for video saliency modeling and discovers that the former can acquire close or even better effect than ConvLSTM. STRA-Net [23] proposes a kind of two-stream model, the motion flow and appearance can couple through dense residual cross-connections at various layers, meanwhile, multiple local attentions can be utilized to enhance the integration of the temporal-spatial features and then conduct the final prediction of saliency map through ConvGRU and global attention. SalSAC [40] improves the robustness of network through shuffled attention module, and the

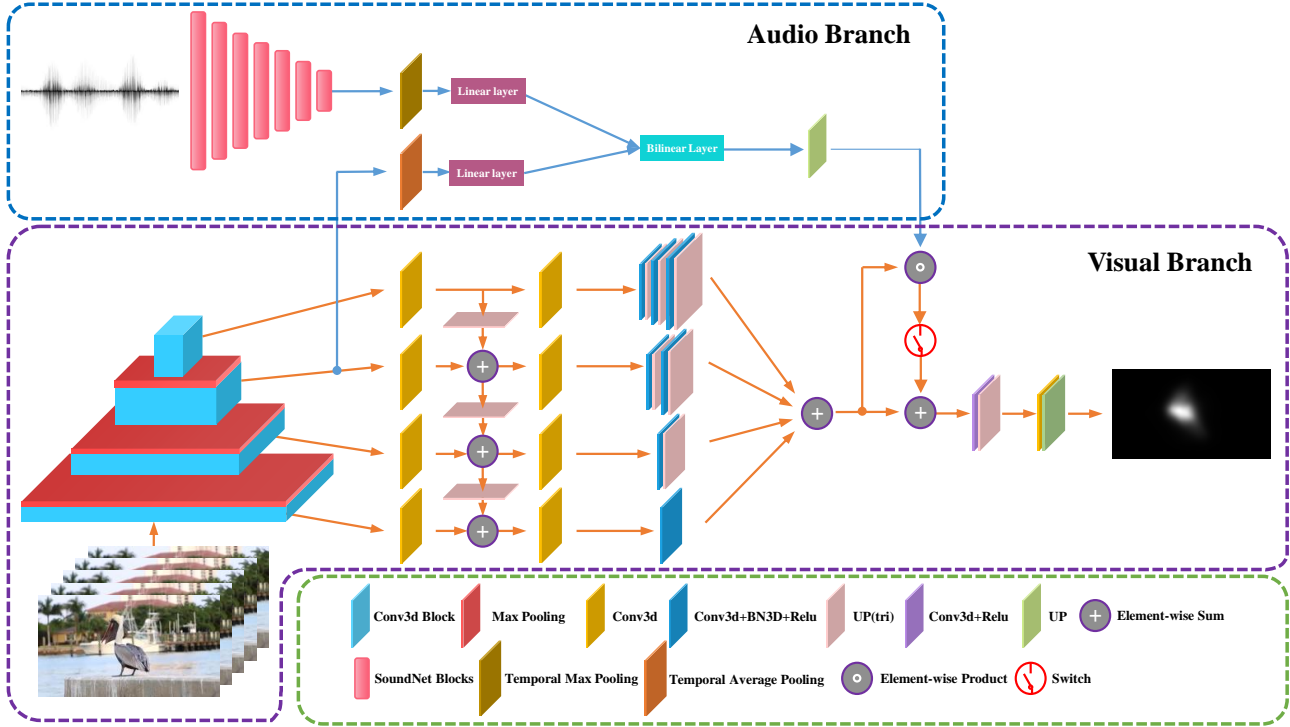


Figure 2. The overall architecture of the TSFP-Net (Notes: UP(tri) means trilinear upsampling, UP means bilinear upsampling)

correlation-based ConvLSTM is employed to balance the change of static image feature for previous frame and current frame. ESAN-VSP [6] adopts a multi-scale deformable convolutional alignment network (MDAN) to align the feature of adjacent frames and then predicts the video motion information through Bi-ConvLSTM. UNISAL [14] is a unified image and video saliency detection model, which can extract the static feature through MobileNet v2 [35] and determine whether to predict the temporal information through the ConvGRU connected by the residual of the controllable switch. In addition, it also adopts the domain adaptation technology to realize the high-precision saliency detection of various video datasets and image datasets.

2.2. The Latest 3D Video Saliency Detection Networks

RMDN [3] utilizes C3D [37] to extract the temporal-spatial features and then aggregates time information through LSTM. TASED-Net [28] adopts S3D network [41] as encoder and the decoder uses 3D deconvolution and unpooling so as to continuously enlarge the image to obtain the saliency map. The unpooling layer adopts *Auxiliary pooling* to fill the feature acquired from the decoder to the activated position corresponding to the maxpooling layer of the encoder. SalGradNet [4] delivers the multi-scale features output by 3D encoder to a conspicuity net for decoding separately and then combines all the decoded feature maps

to obtain the final saliency map. ViNet [19] adopts a 3D encoder-decoder structure in a 2D U-Net like fashion so that the decoding features of various layers can be constantly concatenated with the corresponding feature of encoder in the temporal dimension, and then, the video saliency detection results can be obtained through continuous 3D convolution and trilinear upsampling.

2.3. Audio-Video Saliency Prediction

Some recent studies have begun to explore the impact of the combination of vision and hearing on saliency. SoundNet [1] uses a large amount of unlabeled sound data and video data, and uses a pre-trained visual model for self-supervised learning to obtain an acoustic representation. STAVIS [38] performs a spatial sound source localization through SoundNet combined visual features in SUSiNet [22], and concatenates the feature maps obtained through sound source localization and visual output feature maps to merge and output the saliency map. AViNet [19] uses three different methods to fuse the advanced features of the SoundNet output with the deepest features of the ViNet encoder, and then performs audio-video saliency prediction.

We design a 3D fully convolutional encoder-decoder architecture for video saliency detection since the huge defect existed in the model designed in the 2D network described in the preceding part of the paper. Different from the above mentioned 3D network, our network completely utilizes the

3D convolutional layer and trilinear upsampling layer. Our network is the first to build temporal-spatial feature pyramid in the field of video saliency and aggregate deep semantic features in each layer of feature maps in the feature pyramid. Through the hierarchical decoding of temporal-spatial features at different scales, we obtain the detection results of video saliency that are significantly superior than existing networks. At the same time, in order to make full use of sound information and visual information for audio-video saliency detection, we fuse sound information and visual information for sound source localization, and connect residuals with the features of the original visual network in the form of attention and then obtain audio-video saliency model.

3. The Proposed Methods

3.1. Network Structure

The overall architecture of our model is shown in Figure 2. For purely visual branch TSFP-Net, since the saliency of any frame is determined by several frames in the past, hence, the network inputs T frames at one time, and finally outputs a saliency map of the last frame of a T frames video clip. That is, given the input video clip $\{I_{t-T+1}, \dots, I_t\}$, the S3D[41] encoder performs temporal-spatial feature aggregation through 3D convolution and maxpooling so as to obtain the temporal-spatial features of different scales, then, the top-down path enhancement integrates deep temporal-spatial semantic features into shallow feature maps of different scales to establish the temporal-spatial feature pyramid, next, the temporal-spatial features with multi-scale semantic information are decoded hierarchically. The shallow features have smaller receptive fields, which are utilized to detect the small salient objects, and the deep layer features have the larger receptive fields, which are utilized to detect the large salient objects. As a result, the features of different levels are continuously decoded and upsampled so as to obtain the features with same temporal-spatial and channel dimension. These features are summed element by element, and the time and channel dimensions are reduced through the 3D convolution of the output layer, finally, the saliency map S_t at time t is obtained through the sigmoid activation function.

For the combination of audio-video saliency, we input the sound waves of the T-frame clips corresponding to the visual network, obtaining the sound representation through SoundNet. We use the bilinear transformation to fuse the features of the base3 output of the S3D encoder with the sound representation, and then upsample to obtain the attention map. The attention map with the sound information and the integrated visual feature map are combined by elementwise product and residual connection summation to obtain the features of the fused sound information. And the final audio-video saliency map is obtained through the out-

put network.

In this way, in the form of a sliding window, each time we insert a new frame and delete the first frame, leaving the length of the video clip in the window as T , we can perform frame-by-frame video saliency detection, by doing so, all saliency results of the T frames and subsequent frames of each video can be detected. For the first $T - 1$ frames, we can obtain the saliency maps by roughly reversely playing the video frame of first $2T - 1$ frames and putting them into the sliding window.

3.2. Loss Function

The training of the video saliency network is a regression problem, which aims to make the distribution of the output saliency map consistent with the ground truth. In the past, a large number of video saliency models adopted *Kullback-Leibler (KL) divergence* as a loss function to train the model and achieved good results. However, there are multiple metrics that evaluate the saliency from different aspects, among them, the *Linear Correlation Coefficient (CC)* and the *Normalized Scanpath Saliency (NSS)* seem to be more reliable to evaluate the quality of the saliency map. We take the weighted summation of the above KL, CC and NSS to represent the final loss function and the subsequent ablation studies prove that the weighted summation of the three losses achieve better results than just using KL loss.

Assuming that the predicted saliency map is $S \in [0, 1]$, the labeled binary fixation map is $F \in \{0, 1\}$, and the ground truth saliency map generated by the fixation map is $G \in [0, 1]$, the final loss function can be expressed as:

$$L(S, F, G) = L_{KL}(S, G) + \alpha_1 L_{CC}(S, G) + \alpha_2 L_{NSS}(S, F)$$

Where $\alpha_1 = 0.5$, $\alpha_2 = 0.1$. L_{KL} , L_{CC} and L_{NSS} respectively signify the loss of *Kullback-Leibler (KL) divergence*, the *Linear Correlation Coefficient (CC)*, and the *Normalized Scanpath Saliency (NSS)*. The calculation formulas of them are as follows:

$$L_{KL}(S, G) = \sum_x G(x) \ln \frac{G(x)}{S(x)} \quad (1)$$

$$L_{CC}(S, G) = -\frac{\text{cov}(S, G)}{\rho(S)\rho(G)} \quad (2)$$

$$L_{NSS}(S, F) = -\frac{1}{N} \sum_x s(x)F(x), \quad (3)$$

$$\left(s(x) = \frac{S(x) - \mu(S(x))}{\rho(S(x))} \right)$$

Where $\sum_x(\cdot)$ represents summing all the pixels, $\text{cov}(\cdot)$ represents the covariance, $\mu(\cdot)$ represents the mean and $\rho(\cdot)$ represents the variance.

4. Experimental Results

4.1. Datasets

Just like most video saliency studies, we evaluate our method on the three most commonly used video

saliency datasets, which are DHF1K [39], Hollywood-2 [27], and UCF-sports [27]. At the same time, we evaluate our model on six audio-video saliency datasets: DIEM [30], Coutrot1 [11][12], Coutrot2 [11][12], AVAD [29], ETMD [21], SumMe [16].

DHF1K dataset contains 1000 videos collected from spanning a large range of scenes, motions, object types, and complex background, which is the largest and the most diverse video saliency dataset so far. It consists of 600 videos for training, 100 videos for validation, and 300 videos for testing. For a fair comparison, the first 700 videos publicly provide ground truth for training and validation, while, the rest 300 videos do not provide ground truth, therefore, the experimental results shall be submitted to the evaluation server for blind assessment, which is different from the other datasets. Since the variety of this dataset is the most complicated, we conduct our experiments and ablation studies mainly based on it.

Hollywood-2 dataset contains 1,707 videos, which can be divided into 6,659 short video clips for training and testing, among them, the training set consists of 3,100 clips and the test set consists of 3,559 clips. The dataset is a task-driven video saliency dataset, mainly focusing on human actions in movies scenes.

UCF-sports dataset contains 150 video clips taken from the UCF Sport Action Dataset [33], mainly emphasizing on human actions in sports, it is divided into 103 video clips for training and 47 video clips for testing.

DIEM consists of 81 movie clips of varying genres. They source from publicly accessible repositories, it consists of 64 training videos and 17 test videos.

Coutrot datasets are split into Coutrot1 and Coutrot2. Coutrot1 contains 60 clips with dynamic natural scenes split into 4 visual categories. Coutrot2 contains 15 clips of 4 persons in a meeting and the corresponding eye-tracking data from 40 persons.

AVAD dataset contains 45 short clips of 5-10 sec duration with several audio-visual scenes.

ETMD dataset contains 12 videos from six different hollywood movies.

SumMe dataset contains 25 unstructured videos, which are acquired in a controlled psychological experiment.

4.2. Experimental Setup

In order to train TSFP-Net, we first initialize our encoder using the S3D model pre-trained on Kinetics. In the DHF1K dataset, we adopt standard division of training set and validation set to train our model, T continuous video frames are randomly selected from each video in each time, each frame is resized to 192×352 , the batchsize is set to 16 videos during the training, restricted by the memory, we can only deal with 4 videos each time, so we accumulate the gradient and update the model parameters every other 4 steps. We use the Adam optimizer, the initial learning rate

is set to 0.0001, and the learning rate is reduced by 10 times at the 22nd, 25th, and 26th epochs respectively. We train 26 epochs in total, and use early stopping in the DHF1K validation set to save the model parameters corresponding to the largest NSS result on the validation set. Due to the excessive number of images in the validation set, we only use the first 80 frames of each video for validation during the training process.

As for Hollywood-2 and UCF-sports datasets, we use the models trained on DHF1K to finetune the models separately, since these two datasets contain a large amount of video clips that are less than T , for all video clips less than T in the training set, we first repeat the first frame $T - 1$ times in front, we adopt early stopping on the test set of these two datasets.

In order to train TSFP-Net (with audio), we first use the model pre-trained in DHF1K to initialize the visual branch and finetune on six audio-video saliency datasets without adding sound, and then add sound data to train the audio-video saliency model. The three different splits used in the datasets are the same as [38], and we evaluate the average metrics of different splits.

Evaluation metrics. We use the most commonly used metrics in the DHF1K benchmark to evaluate our model for DHF1K dataset. These include (i) Normalized Scanpath Saliency (NSS), (ii) Linear Correlation Coefficient (CC), (iii) Similarity (SIM), (iv) Area Under the Curve by Judd (AUC-J), and (v) Shuffled-AUC (s-AUC). For all these metrics, the larger, the better. For other datasets and ablation studies, we use AUC-J, SIM, CC and NSS metrics.

4.3. Evaluation on DHF1K

DHF1K is adopted as the preferred dataset for ablation study and evaluation of test set. We change the length of T to 16, 32, and 48 respectively to train our model and observe the results on the DHF1K validation set. The experimental results are shown in Table 1. We discover that when T is 32, the performance is the best, because it obtains the highest AUC-J, CC and NSS.

Clip length (T)	AUC-J	SIM	CC	NSS
16	0.916	0.392	0.500	2.876
32	0.919	0.397	0.529	3.009
48	0.917	0.398	0.526	2.990

Table 1. The experimental results of DHF1K validation set while training at different clip length (T).

Next, we submit the results of our model to the evaluation server of DHF1K test set. The results for TSFP-Net and all other state-of-the-art methods [4, 14, 19, 20, 23, 25, 28, 39, 40] on DHF1K test set are shown in Table 2. We discover that our model is significantly better than other state-of-the-art methods, especially, NSS, CC and AUC-J make remarkable gains. Although s-AUC and SIM fail to rank the

first, they make the top three. In particular, according to [5], s-AUC assumes center bias has not been modeled, and penalizes models when they have center bias, however, center bias itself conforms to the behavior of watching freely with human eyes, compared with s-AUC, so AUC is more suitable to evaluate the performance of video saliency model. Whereas, SIM penalizes models with false negatives significantly more than false positives, in terms of evaluating, it is inferior to NSS and CC that treat false positives and false negatives symmetrically. Consequently, NSS and CC are believed to be related to human eye's visual attention most and recommended to evaluate the saliency model [5], compared with other methods, we make a huge breakthrough in terms of NSS and CC. Meanwhile, as known as in Table 2, the models based on 3D fully convolutional encoder-decoder are mostly superior to the 2D models based on LSTM [14, 20, 23, 25, 39, 40], which is related to the defects of the 2D network that we analyzed previously and the simultaneous temporal-spatial aggregation of 3D convolution. Our model is currently the most powerful 3D full convolutional encoder-decoder and video saliency network so far, which proves the effectiveness of our method.

Method \ Metrics	NSS	CC	SIM	AUC-J	s-AUC
Method	NSS	CC	SIM	AUC-J	s-AUC
DeepVS [20]	1.911	0.344	0.256	0.856	0.583
ACLNet [39]	2.354	0.434	0.315	0.890	0.601
SalEMA [25]	2.574	0.449	0.466	0.890	0.667
STRA-Net [23]	2.558	0.458	0.355	0.895	0.663
TASED-Net [28]	2.667	0.470	0.361	0.895	0.712
SalSAC [40]	2.673	0.479	0.357	0.896	0.697
UNISAL [14]	2.776	0.490	0.390	0.901	0.691
SalGradNet [4]	2.781	0.497	0.406	0.901	0.699
ViNet [19]	2.872	0.511	0.381	0.908	0.729
TSFP-Net	2.966	0.517	0.392	0.912	0.723

Table 2. Comparison of the saliency metrics on DHF1K test set for TSFP-Net and other state-of-the-art methods (The best scores are shown in red and second best scores in blue).

We visualize the saliency maps generated through TSFP-Net from DHF1K validation set and compare it with other state-of-the-art methods, which is shown in Figure 3. Since TASED-Net has been updated to TASED-Net v2 and the code is open source, the NSS on the DHF1K test set can be up to 2.797, as a result, we compare TSFP-Net with the two most powerful models recently published: TASED-Net v2 and UNISAL. It can be seen that our model has great advantages. Firstly, the saliency maps generated by our method are more concentrated and have a smaller area that is closer to ground truth, while the saliency maps of the other two methods are more scattered. Secondly, our method usually does not produce false detections and missed detections, while the other two methods have more obvious false detections and missed detections. As shown in Figure 3 (a), the other two methods produce redundant detections, in

Methods	Runtime(s)
DeepVS [20]	0.05
ACLNet [39]	0.02
SalEMA [25]	0.01
STRA-Net [23]	0.02
TASED-Net [28]	0.06
SalSAC [40]	0.02
UNISAL [14]	0.009
SalGradNet [4]	0.03
ViNet [19]	0.016
TSFP-Net	0.011

Table 3. Runtime comparison for TSFP-Net and other state-of-the-art methods.

Figure 3 (c), only our model can accurately detect fishing hooks, TASED-Net v2 produces redundant detections, and UNISAL is completely wrong.

We also compare the runtime of our model with other state-of-the-art methods. We test our model on a NVIDIA RTX 2080 Ti, which take about 0.011s to generate a saliency map. The running time comparison with other methods is shown in Table 3. As can be seen that not only the accuracy of our model greatly exceed the state-of-the-art methods, but also the speed of generating the saliency map is fast enough.

4.4. Evaluation on Other Datasets

We also evaluate the performance of our model on Hollywood-2 and UCF-sports. We observe that these two datasets are task-driven video saliency datasets, and there are a large number of video clips with less than 32 frames, and even Hollywood-2 has many video clips with only 1 or 2 frames, and the difference between two adjacent frames of all video clips is very obvious. Reverse playback of the video itself can change the video saliency, on the large-scale DHF1K dataset, since the length of video clips is long enough (several hundred frames), the images are extracted according to the appropriate frame rate, and the types of videos are diverse, the impact of the reverse playback can be mitigated to produce normal saliency results in the previous frames of the video.

However, we reveal that in these two datasets, the saliency results of the previous frame obtained from reverse playback are very poor. As a result, we don't adopt reverse playback to predict the saliency of the previous frame during the test set. Specifically, in terms of the video frames that are less than T , we supplement $T-1$ frames in front and obtain the saliency frame by frame through order of play; in terms of the clip length that is between T and $2T-1$, we repeat the first frame and supplement the video clips to $2T-1$, then, we predict the saliency frame by frame after the T frames; as for the clip length that is greater or equal to $2T-1$, we directly predict the saliency frame by frame of all frames after the T frames. The comparison results of

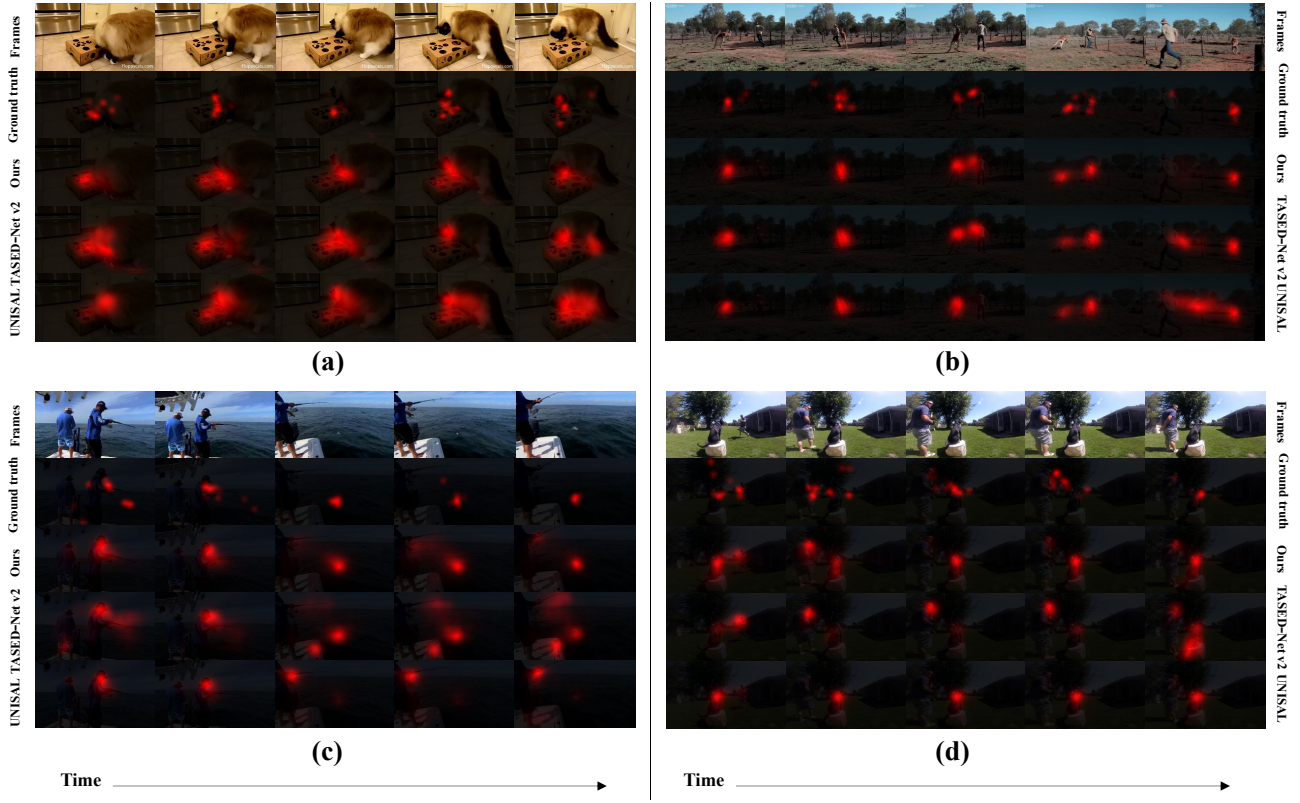


Figure 3. The comparison of visualization results of saliency maps for TSFP-Net and other two state-of-the-art methods, as we can see from the figure, TSFP-Net is significantly superior to TASED-Net v2 and UNISAL, the generated saliency maps are more dense, and there is basically no false detection and missed detection, while the other two methods have obvious false detection and missed detection.

Method	Dataset	Hollywood-2				UCF-sports			
		AUC-J	SIM	CC	NSS	AUC-J	SIM	CC	NSS
DeepVS [20]		0.887	0.356	0.446	2.313	0.870	0.321	0.405	2.089
ACLNet [39]		0.913	0.542	0.623	3.086	0.897	0.406	0.510	2.567
SalEMA [25]		0.919	0.487	0.613	3.186	0.906	0.431	0.544	2.638
STRA-Net [23]		0.923	0.536	0.662	3.478	0.910	0.479	0.593	3.018
TASED-Net [28]		0.918	0.507	0.646	3.302	0.899	0.469	0.582	2.920
SalSAC [40]		0.931	0.529	0.670	3.356	0.926	0.534	0.671	3.523
UNISAL [14]		0.934	0.542	0.673	3.901	0.918	0.523	0.644	3.381
SalGradNet [4]		0.927	0.558	0.668	3.426	0.913	0.493	0.594	3.001
ViNet [19]		0.930	0.550	0.693	3.730	0.924	0.522	0.673	3.620
TSFP-Net		0.936	0.571	0.711	3.910	0.923	0.561	0.685	3.698

Table 4. The comparison of saliency metrics for TSFP-Net and other state-of-the-art methods on Hollywood-2 test set and UCF-sports test set (The best scores are shown in red and second best scores in blue).

our method on the Hollywood-2 and UCF-sports test sets obtained in this way and other state-of-the-art methods are shown in Table 4, it can be seen that our model is also highly superior to other methods on these two datasets.

We also evaluated the results of TSFP-Net and TSFP-

Net (with audio) on six audio-video saliency datasets, and the performance comparisons with other methods are shown in Table 5 and Table 6. It can be seen that our two models are much better than all the state-of-the-art methods on most datasets. The results of TSFP-Net (with audio) are

Method	Dataset	DIEM				Coutrot1				Coutrot2			
		AUC-J	SIM	CC	NSS	AUC-J	SIM	CC	NSS	AUC-J	SIM	CC	NSS
ACLNet [39]		0.869	0.427	0.522	2.02	0.850	0.361	0.425	1.92	0.926	0.322	0.448	3.16
TASED-Net [28]		0.881	0.461	0.557	2.16	0.867	0.388	0.479	2.18	0.921	0.314	0.437	3.17
STAVIS [38]		0.883	0.482	0.579	2.26	0.868	0.393	0.472	2.11	0.958	0.511	0.734	5.28
ViNet [19]		0.898	0.483	0.626	2.47	0.886	0.423	0.551	2.68	0.950	0.466	0.724	5.61
AViNet(B) [19]		0.899	0.498	0.632	2.53	0.889	0.425	0.560	2.73	0.951	0.493	0.754	5.95
TSFP-Net		0.905	0.529	0.649	2.63	0.894	0.451	0.570	2.75	0.957	0.516	0.718	5.30
TSFP-Net (with audio)		0.906	0.527	0.651	2.62	0.895	0.447	0.571	2.73	0.959	0.528	0.743	5.31

Table 5. Comparison results on the DIEM, Coutrot1 and Coutrot2 test sets (bold is the best).

Method	Dataset	AVAD				ETMD				SumMe			
		AUC-J	SIM	CC	NSS	AUC-J	SIM	CC	NSS	AUC-J	SIM	CC	NSS
ACLNet [39]		0.905	0.446	0.58	3.17	0.915	0.329	0.477	2.36	0.868	0.296	0.379	1.79
TASED-Net [28]		0.914	0.439	0.601	3.16	0.916	0.366	0.509	2.63	0.884	0.333	0.428	2.1
STAVIS [38]		0.919	0.457	0.608	3.18	0.931	0.425	0.569	2.94	0.888	0.337	0.422	2.04
ViNet [19]		0.928	0.504	0.694	3.82	0.928	0.409	0.569	3.06	0.898	0.345	0.466	2.40
AViNet(B) [19]		0.927	0.491	0.674	3.77	0.928	0.406	0.571	3.08	0.897	0.343	0.463	2.41
TSFP-Net		0.931	0.530	0.688	3.79	0.932	0.433	0.576	3.09	0.894	0.362	0.463	2.28
TSFP-Net (with audio)		0.932	0.521	0.704	3.77	0.932	0.428	0.576	3.07	0.894	0.360	0.464	2.30

Table 6. Comparison results on the AVAD, ETMD and SumMe test sets (bold is the best).

only slightly better than TSFP-Net (such as a slight increase in the AUC-J metric), indicating that visual information is dominant in the prediction of audio-video saliency.

4.5. Ablation Studies

We first prove that the multi-scale temporal-spatial feature pyramid constructed by top-down path enhancement and hierarchical decoding are effective and important for video saliency prediction.

Firstly, we only use the hierarchical decoder and do not build the temporal-spatial feature pyramid, we only change the channel dimensions of the output multi-scale temporal-spatial features through $1 \times 1 \times 1$ convolution to make the feature channels input into the hierarchical decoder consistent, after that, the features directly input the hierarchical decoder for decoding and are integrated to obtain the saliency map, this configuration is TSFP-Net (only multi-

level). Secondly, we delete the hierarchical decoder and only adopt the deepest features of the encoder for decoding to get saliency, the configuration is TSFP-Net (only final-level). The results on the validation set of DHF1K for different network structures are shown in Table 7. We reveal that the results of hierarchical decoding for different layer's are significantly better than that obtained using only deepest layer's features, and adding top-down path enhancement to construct a semantic temporal-spatial feature pyramid combined with hierarchical decoding has the best effect. Compared to TASED-Net [28], which adopts 3D deconvolution and unpooling, our TSFP-Net (only final-level) only adopts 3D convolution and trilinear upsampling, the NSS result on the validation set of DHF1K is 2.787, which is better than that of TASED-Net, which is 2.706. It indicates that deconvolution and unpooling not only rely too much on the maxpooling layer in the encoder, which leads to the inability to freely design the network structure, but also limits the learning ability of the network to some extent.

We also compare the effects of different loss functions on network performance, the results are shown in Table 8. We prove that the adoption of the weighted summation of three losses can obtain better performance than using KL loss alone.

Different Architecture	NSS	CC	AUC-J	SIM
TSFP-Net (only final-level)	2.7868	0.5010	0.9121	0.3860
TSFP-Net (only multi-level)	2.8857	0.5097	0.9156	0.3819
TSFP-Net	3.0086	0.5290	0.9188	0.3975

Table 7. Performance comparison for TSFP-Net with different network structures on the validation set of DHF1K.

Different Loss	NSS	CC	AUC-J	SIM
TSFP-Net (only KL loss)	2.9876	0.5287	0.9186	0.3927
TSFP-Net	3.0086	0.5290	0.9188	0.3975

Table 8. Performance comparison for TSFP-Net with different loss functions on the validation set of DHF1K.

coding is conducted to the multi-scale temporal-spatial features, and finally a video saliency detection model that is significantly superior to all state-of-the-art methods is obtained. Our performances on three purely visual video saliency benchmarks and six audio-video saliency benchmarks prove the effectiveness of our method, and our model is real-time.

Acknowledgments

This work is supported by the National Key Technologies R&D Program of China (Grant No. 2016YFB0500505), National Natural Science Foundation of China (NSFC) under grants No. 61375025, 61075011 and 60675018, and also the Scientific Research Foundation for the Returned Overseas Chinese Scholars from the State Education Ministry of China.

References

- [1] Yusuf Aytar, Carl Vondrick, and Antonio Torralba. Soundnet: Learning sound representations from unlabeled video. *arXiv preprint arXiv:1610.09001*, 2016. [3](#)
- [2] Vijay Badrinarayanan, Alex Kendall, and Roberto Cipolla. Segnet: A deep convolutional encoder-decoder architecture for image segmentation. *IEEE Transactions on Pattern Analysis and Machine Intelligence*, 39(12):2481–2495, 2017. [2](#)
- [3] Loris Bazzani, Hugo Larochelle, and Lorenzo Torresani. Recurrent mixture density network for spatiotemporal visual attention. *arXiv preprint arXiv:1603.08199*, 2016. [3](#)
- [4] Giovanni Bellitto, Federica Proietto Salanitri, Simone Palazzo, Francesco Rundo, Daniela Giordano, and Concetto Spampinato. Video saliency detection with domain adaption using hierarchical gradient reversal layers. *arXiv preprint arXiv:2010.01220*, 2020. [1, 3, 5, 6, 7](#)
- [5] Zoya Bylinskii, Tilke Judd, Aude Oliva, Antonio Torralba, and Frédo Durand. What do different evaluation metrics tell us about saliency models? *IEEE Transactions on Pattern Analysis and Machine Intelligence*, 41(3):740–757, 2018. [6](#)
- [6] Jin Chen, Huihui Song, Kaihua Zhang, Bo Liu, and Qingshan Liu. Video saliency prediction using enhanced spatiotemporal alignment network. *Pattern Recognition*, 107615:1–12, 2021. [3](#)
- [7] Liang-Chieh Chen, George Papandreou, Iasonas Kokkinos, Kevin Murphy, and Alan L Yuille. Semantic image segmentation with deep convolutional nets and fully connected crfs. *arXiv preprint arXiv:1412.7062*, 2014. [2](#)
- [8] Liang-Chieh Chen, George Papandreou, Iasonas Kokkinos, Kevin Murphy, and Alan L Yuille. Deeplab: Semantic image segmentation with deep convolutional nets, atrous convolution, and fully connected crfs. *IEEE Transactions on Pattern Analysis and Machine Intelligence*, 40(4):834–848, 2017. [2](#)
- [9] Liang-Chieh Chen, George Papandreou, Florian Schroff, and Hartwig Adam. Rethinking atrous convolution for semantic image segmentation. *arXiv preprint arXiv:1706.05587*, 2017. [2](#)
- [10] Liang-Chieh Chen, Yukun Zhu, George Papandreou, Florian Schroff, and Hartwig Adam. Encoder-decoder with atrous separable convolution for semantic image segmentation. In *Proceedings of the European Conference on Computer Vision (ECCV)*, pages 801–818, 2018. [2](#)
- [11] Antoine Coutrot and Nathalie Guyader. How saliency, faces, and sound influence gaze in dynamic social scenes. *Journal of Vision*, 14(8):5–5, 2014. [5](#)
- [12] Antoine Coutrot and Nathalie Guyader. Multimodal saliency models for videos. In *From Human Attention to Computational Attention*, pages 291–304. Springer, 2016. [5](#)
- [13] Alexey Dosovitskiy, Philipp Fischer, Eddy Ilg, Philip Hausser, Caner Hazirbas, Vladimir Golkov, Patrick Van Der Smagt, Daniel Cremers, and Thomas Brox. Flownet: Learning optical flow with convolutional networks. In *Proceedings of the IEEE International Conference on Computer Vision*, pages 2758–2766, 2015. [2](#)
- [14] Richard Droste, Jianbo Jiao, and J Alison Noble. Unified image and video saliency modeling. In *European Conference on Computer Vision*, pages 419–435. Springer, 2020. [3, 5, 6, 7](#)
- [15] Fahad Fazal Elahi Guraya, Faouzi Alaya Cheikh, Alain Tremeau, Yubing Tong, and Hubert Konik. Predictive saliency maps for surveillance videos. In *2010 Ninth International Symposium on Distributed Computing and Applications to Business, Engineering and Science*, pages 508–513. IEEE, 2010. [1](#)
- [16] Michael Gygli, Helmut Grabner, Hayko Riemenschneider, and Luc Van Gool. Creating summaries from user videos. In *European Conference on Computer Vision (ECCV)*, pages 505–520. Springer, 2014. [5](#)
- [17] Hadi Hadizadeh and Ivan V Bajić. Saliency-aware video compression. *IEEE Transactions on Image Processing*, 23(1):19–33, 2013. [1](#)
- [18] Xun Huang, Chengyao Shen, Xavier Boix, and Qi Zhao. Salicon: Reducing the semantic gap in saliency prediction by adapting deep neural networks. In *Proceedings of the IEEE International Conference on Computer Vision*, pages 262–270, 2015. [2](#)
- [19] Samyak Jain, Pradeep Yarlagadda, Ramanathan Subramanian, and Vineet Gandhi. Avinet: Diving deep into audio-visual saliency prediction. *arXiv preprint arXiv:2012.06170*, 2020. [3, 5, 6, 7, 8](#)
- [20] Lai Jiang, Mai Xu, Tie Liu, Minglang Qiao, and Zulin Wang. Deepvs: A deep learning based video saliency prediction approach. In *Proceedings of the European Conference on Computer Vision (ECCV)*, pages 602–617, 2018. [2, 5, 6, 7](#)
- [21] Petros Koutras and Petros Maragos. A perceptually based spatio-temporal computational framework for visual saliency estimation. *Signal Processing: Image Communication*, 38:15–31, 2015. [5](#)
- [22] Petros Koutras and Petros Maragos. Susinet: See, understand and summarize it. In *Proceedings of the IEEE/CVF Conference on Computer Vision and Pattern Recognition Workshops*, pages 809–819, 2019. [3](#)
- [23] Qixia Lai, Wenguan Wang, Hanqiu Sun, and Jianbing Shen. Video saliency prediction using spatiotemporal residual attentive networks. *IEEE Transactions on Image Processing*, 29:1113–1126, 2019. [2, 5, 6, 7](#)

[24] Guosheng Lin, Anton Milan, Chunhua Shen, and Ian Reid. Refinenet: Multi-path refinement networks for high-resolution semantic segmentation. In *Proceedings of the IEEE Conference on Computer Vision and Pattern Recognition*, pages 1925–1934, 2017. 2

[25] Panagiotis Linardos, Eva Mohedano, Juan Jose Nieto, Noel E O’Connor, Xavier Giro-i Nieto, and Kevin McGuinness. Simple vs complex temporal recurrences for video saliency prediction. *arXiv preprint arXiv:1907.01869*, 2019. 1, 2, 5, 6, 7

[26] Jonathan Long, Evan Shelhamer, and Trevor Darrell. Fully convolutional networks for semantic segmentation. In *Proceedings of the IEEE Conference on Computer Vision and Pattern Recognition*, pages 3431–3440, 2015. 2

[27] Stefan Mathe and Cristian Sminchisescu. Actions in the eye: Dynamic gaze datasets and learnt saliency models for visual recognition. *IEEE Transactions on Pattern Analysis and Machine Intelligence*, 37(7):1408–1424, 2014. 5

[28] Kyle Min and Jason J Corso. Tased-net: Temporally-aggregating spatial encoder-decoder network for video saliency detection. In *Proceedings of the IEEE/CVF International Conference on Computer Vision*, pages 2394–2403, 2019. 1, 2, 3, 5, 6, 7, 8

[29] Xiongkuo Min, Guangtao Zhai, Ke Gu, and Xiaokang Yang. Fixation prediction through multimodal analysis. *ACM Transactions on Multimedia Computing, Communications, and Applications (TOMM)*, 13(1):1–23, 2016. 5

[30] Parag K Mital, Tim J Smith, Robin L Hill, and John M Henderson. Clustering of gaze during dynamic scene viewing is predicted by motion. *Cognitive Computation*, 3(1):5–24, 2011. 5

[31] Tam V Nguyen, Mengdi Xu, Guangyu Gao, Mohan Kankanhalli, Qi Tian, and Shuicheng Yan. Static saliency vs. dynamic saliency: a comparative study. In *Proceedings of the 21st ACM International Conference on Multimedia*, pages 987–996, 2013. 1

[32] Joseph Redmon, Santosh Divvala, Ross Girshick, and Ali Farhadi. You only look once: Unified, real-time object detection. In *Proceedings of the IEEE Conference on Computer Vision and Pattern Recognition*, pages 779–788, 2016. 2

[33] Mikel D Rodriguez, Javed Ahmed, and Mubarak Shah. Action mach a spatio-temporal maximum average correlation height filter for action recognition. In *2008 IEEE Conference on Computer Vision and Pattern Recognition*, pages 1–8, 2008. 5

[34] Olaf Ronneberger, Philipp Fischer, and Thomas Brox. U-net: Convolutional networks for biomedical image segmentation. In *International Conference on Medical Image Computing and Computer-assisted Intervention*, pages 234–241. Springer, 2015. 2

[35] Mark Sandler, Andrew Howard, Menglong Zhu, Andrey Zhmoginov, and Liang-Chieh Chen. Mobilenetv2: Inverted residuals and linear bottlenecks. In *Proceedings of the IEEE Conference on Computer Vision and Pattern Recognition*, pages 4510–4520, 2018. 3

[36] Xingjian Shi, Zhourong Chen, Hao Wang, Dit-Yan Yeung, Wai-Kin Wong, and Wang-chun Woo. Convolutional lstm network: A machine learning approach for precipitation nowcasting. *arXiv preprint arXiv:1506.04214*, 2015. 1

[37] Du Tran, Lubomir Bourdev, Rob Fergus, Lorenzo Torresani, and Manohar Paluri. Learning spatiotemporal features with 3d convolutional networks. In *Proceedings of the IEEE International Conference on Computer Vision*, pages 4489–4497, 2015. 3

[38] Antigoni Tsiami, Petros Koutras, and Petros Maragos. Stavis: Spatio-temporal audiovisual saliency network. In *Proceedings of the IEEE/CVF Conference on Computer Vision and Pattern Recognition*, pages 4766–4776, 2020. 1, 3, 5, 8

[39] Wenguan Wang, Jianbing Shen, Fang Guo, Ming-Ming Cheng, and Ali Borji. Revisiting video saliency: A large-scale benchmark and a new model. In *Proceedings of the IEEE Conference on Computer Vision and Pattern Recognition*, pages 4894–4903, 2018. 1, 2, 5, 6, 7, 8

[40] Xinyi Wu, Zhenyao Wu, Jinglin Zhang, Lili Ju, and Song Wang. Salsac: a video saliency prediction model with shuffled attentions and correlation-based convlstm. In *Proceedings of the AAAI Conference on Artificial Intelligence*, volume 34, pages 12410–12417, 2020. 1, 2, 5, 6, 7

[41] Saining Xie, Chen Sun, Jonathan Huang, Zhuowen Tu, and Kevin Murphy. Rethinking spatiotemporal feature learning: Speed-accuracy trade-offs in video classification. In *Proceedings of the European Conference on Computer Vision (ECCV)*, pages 305–321, 2018. 3, 4

[42] Tong Yubing, Faouzi Alaya Cheikh, Fahad Fazal Elahi Guraya, Hubert Konik, and Alain Tréneau. A spatiotemporal saliency model for video surveillance. *Cognitive Computation*, 3(1):241–263, 2011. 1

[43] Shiping Zhu, Chang Liu, and Ziyao Xu. High-definition video compression system based on perception guidance of salient information of a convolutional neural network and hevc compression domain. *IEEE Transactions on Circuits and Systems for Video Technology*, 30(7):1946–1959, 2019. 1